The Astrophysical Journal, 695:420–430, 2009 April 10 doi:10.1088/0004-637X/695/1/420

FOUR-FLUID MODEL AND NUMERICAL SIMULATIONS OF MAGNETIC STRUCTURES IN THE HELIOSHEATH

K. Avinash[1], Sean M. Cox, Dastgeer Shaikh, and G. P. Zank
Centre for Space Plasma and Aeronomic Research, University of Alabama, Hunstville, AL 35899, USA
Received 2008 July 14; accepted 2009 January 8; published 2009 March 31

ABSTRACT

The first part of this paper extends the three-fluid model of Avinash & Zank for magnetic structures in the heliosheath to a four-fluid model consisting of electrons, pick-up ions (PUIs), solar wind ions (SWIs), and neutral hydrogen. The PUIs are generated by neutrals via charge exchange with SWI. Since the kinetic pressure of PUI is nearly three to four times the pressure of SWI, these are more suited to mediate small-scale structures in the heliosheath such as magnetic holes (MH)/humps etc. The constant energy exchange between these two fluids drives them nonadiabatic. The PUIs are isothermal ($\gamma = 1$) while SWIs are nonadiabatic with an index $\gamma \approx 1.25$. The four-fluid model captures these effects via a modified equation of state for PUI and SWI. The phase space of time-independent solutions in terms of the Mach numbers of PUI and SWI is constructed to delineate the parameter space which allows structure formation in the heliosheath. The second part of the paper examines the stability of the time-independent solutions computed in the first part by evolving them via a full system of Hall–MHD equations. The simulation results show that these solutions are not quite stable. As the structure propagates it develops growing oscillations in the wings. Concomitantly, there are changes in the amplitude and width of the structure. This instability could be due to local changes in the velocity of the structure and reflects an exchange between the kinetic and magnetic parts of the total energy. Our results about the presence of growing oscillations in the wings of solitary wave solutions are consistent with the recent analysis of MHs in the heliosheth by Burlaga et al. Their analysis also shows evidence for the presence of oscillations and instabilities in the wings of MHs in the heliosheath.

Key words: ISM: general – ISM: magnetic fields – methods: numerical – MHD – plasmas – solar wind – turbulence

Online-only material: color figure

1. INTRODUCTION

Magnetic holes (MHs) are stable stationary magnetic structures seen in the solar wind by spacecraft such as *Helios*, *Ulysses*, and *ACE*. Such structures or magnetic decreases (MDs) as some times they are called (Tsurutani & Ho 1999), have also been observed in interplanetary magnetic fields (Turner et al. 1977; Treumann et al. 1990) and in the Earth's magnetosphere, though with different names (holes, bubbles, or cavities; Sugiura et al. 1969; Luhr & Klocker 1987; Stasiewicz et al. 2001). The scale sizes of the MHs/MDs ranges from a few to hundreds of ion gyro radii (Tsurutani & Ho 1999).

Recently, the magnetic data of *Voyager 1* from the heliosheath has revealed the presence of a rich class of stable magnetic structures. These include, what are believed to be, isolated MHs, a sequence of two or three MHs (i.e., a sequence of two or three successive minima), humps, merged sequences of a hump and a hole etc. The width of these structures, which have minima/maxima of the mean magnetic field in the center, was in the range of 40–100 times the pick-up ion (PUI) gyro radii. Other typical features of these structures are strong nonlinearity (amplitude $\approx$ 70%–80% of the mean field), nearly pressure balanced, traveling almost perpendicular to the mean field, occurrence in high beta plasmas, and magnetic field changes that occur mostly in magnitude with very little or no change in the direction of the magnetic field (linear holes) (L. F. Burlaga et al. 2006, private communication; Burlaga et al. 2007). Interestingly though, in the case of interplanetary space and planetary magnetosheath, MHs may not necessarily have a lack of field rotation (Winterhalter et al. 2000).

These structures must carefully be contrasted with mirror mode (MM) structures which have been detected in planetary magnetosheaths of Jupiter (Erdos & Balogh 1996), Saturn (Tsurutani et al. 1982; Violante et al. 1995), Earth (Tsurutani et al. 1982), and cometary plasmas (Russell et al. 1987; Brinca & Tsurutani 1989). They are generated by an ion instability when $\beta_\perp/\beta_{||} > 1 + 1/\beta_\perp$, where b is the ratio of ion kinetic and magnetic field pressure (Chandrasekhar et al. 1958; Hasegawa 1969; Kivelson & Southwood 1996). The structures are smaller ($\sim$12–30 ion gyro radii), occur in a train of several oscillations of magnetic maxima and minima and have total plasma plus magnetic pressure constant to first order. Mirror mode structures were first investigated by Tsurutani et al. (1982) in the planetary magnetosheaths of Earth, Jupiter, and Saturn. There are little or no angular changes throughout the field decreases/increase (Tsurutani et al. 1982, 1999) and the source of free energy for the instability generating these structures was identified as being due to field line draping (Zwan & Wolf 1976) and perpendicular shock compression. Clearly, the structures analyzed by Burlaga et al. (2007) and considered in this paper (i.e., sequences of two or three successive minima on a much longer length scale) are distinct from mirror mode structures.

Since the first observations in 1977 there have been a number of attempts to understand the origin of stable stationary interplanetary magnetic structures. Initially, because of the observed temperature anisotropy, they were explained in terms of the mirror instability (Winterhalter et al. 1994). Specifically Winterhalter et al. (1994, 1995, 2000) have tried to explain the

[1] Permanent Address: Department of Physics and Astrophysics, University of Delhi, 110007, India.

"linear" (those with small angular changes in the MDs) MHs as mirror mode structures.

However it was shown later that the threshold for the mirror instability is not met for most cases (Franz et al. 2000; Tsurutani et al. 2005). Besides, in cases where MHs are bounded by discontinuities, magnetic mirror instability cannot explain these termination features (Tsurutani & Ho 1999). Tsurutani et al. (2002) have suggested formation of MH/MD due to diamagnetic effects caused by pondermotive force mediated perpendicular heating of ions. Burlaga and Lemaire proposed a current sheet model based on solutions of the Vlasov–Maxwell equations where pressure is balanced by the Lorentz force (Burlaga & Lemaire 1978; Fitzenreiter & Burlaga 1978). Zurbuchen & Jokipii (2002) proposed a model for the formation of MHs based on magnetic reconnection. Other notable attempts to explain the formation of these structures include a model based on wave–wave interactions by Vasquez & Hollweg (1999), and the beam microinstabilities model by Neugebauer et al. (2001). The role of the phase steepened Alfvén waves and the concomitant ion heating due to the pondermotive force in the formation of MHs has been emphasized by Tsurutani et al. (2005). Some authors have identified MHs in terms of the dark soliton solutions of the derivative nonlinear Schrodinger (DNLS) equation (Kennel et al. 1988; Baumgartel 1999; Buti et al. 2001b). Specifically, these theories have suggested that the MH may be identified as a dark soliton solution while the magnetic hump may be identified as a bright soliton solution of the DNLS equation. The stability of dark soliton solutions under full Hall MHD dynamics has also been examined (Baumgartel 1999). However, the DNLS-based approach has been criticized on two grounds. First, the DNLS equation is valid only for parallel or at most quasi-parallel propagation while MHs travel almost perpendicular to the mean magnetic field. Second, the derivation of the DNLS equation is based on a perturbative expansion that assumes $\Delta B/B \ll 1$ and hence is inadequate for structures where $\Delta B/B \leqslant 1$. Furthermore, these theories do not take into account some effects that play an important role in heliospheric dynamics not including for example, the separate roles of PUIs and SWIs, the role of neutrals etc.

Recently, we have proposed a three-fluid solitary wave model (Avinash & Zank 2007) for MHs and humps based on the recent work of McKenzie et al. (2001, 2004), suitably modified to take into account some realistic effects related to interstellar neutrals in the heliosheath. The advantage of this approach is that McKenzie's theory is fully nonlinear and is thus valid for arbitrary values of $\Delta B/B$ and for oblique propagation angles. It thus provides an adequate framework for magnetic structures which have $\Delta B/B \leqslant 1$ and propagate at oblique angles to the magnetic field. The three fluids in the model are electrons, heliosheath ions, and neutrals. It was shown that due to charge exchange, neutrals provide extra momentum and energy sources, which somewhat modifies the simpler ion dynamics of McKenzie et al. Using parameters of the heliosheath, a number of one-dimensional stationary time-independent solutions including holes, humps, linear trains of such structures, quantitatively similar to the *Voyager* observations, were derived.

In this paper, we extend our three-fluid model to include two important effects. First, the interstellar neutrals charge exchange with SWI, and produce PUI along with a population of energetic neutrals. The PUI distribution initially forms a highly unstable ring distribution, which quickly relaxes to a bispherical shell in velocity space (Zank 1999; Williams & Zank 1994; Zank et al. 1996b). Thus, the heliosheath ions, which in our three-fluid model were treated as one fluid, actually consists of two distinct species; PUI and SWI with different roles in the heliosheath. As has been shown (Zank et al. 1996a), the kinetic pressure of PUI is nearly three to four times that of SWI. Hence PUI are more suited to mediate small-scale structures such as shocks, MHs etc in the heliosheath. Burlaga et al. (1994) in fact showed that PUIs provide the primary bulk thermal pressure for pressure-balancedstructures observed by *Voyager* in the heliosphere. Recently *Voyager 2* has crossed the termination shock (Burlaga et al. 2007) and the observations reveal that indeed the solar wind plasma is relatively cool as compared to the PUI plasma.

The energy exchange between PUI and SWI introduces nonadiabatic behavior, which as we shall show here, has important consequences for structure formation in the heliosheath. To capture all these effects, we construct a four-fluid model in which, along with electrons and neutrals, PUI and SWI are treated as two separate fluids.

Second, we examine the stability of our one-dimensional time-independent solutions by evolving them via the full set of time-dependent equations. This is important and has bearing on theories which seek to interpret magnetic structures in terms of soliton solutions. The stability of the DNLS soliton solution has been addressed by Buti et al. (2001a), Baumgartel (1999), and (2003). In these studies the temporal evolution of DNLS solution, a single pulse/solitary wave or the interaction of two solitary wave/DNLS solutions has been examined via Hall–MHD code or a one-dimensional hybrid code. However the results of these studies are somewhat at variance with each other and are rather inconclusive. Buti et al. (2001a) have shown that dark as well as bright DNLS solitons solutions are unstable. These results are inconsistent with the observations of *Voyager 1* which show the presence of long-lived, robust MHs as well as humps (Burlaga et al. 2006). On the other hand, the results of Baumgartel et al. show that the dark soliton is stable while the bright ones are not. These results are partially consistent with the *Voyager 1* observations, which as stated above, show the presence of long-lived MHs as well as humps. Thus, the stability of the DNLS solution as well as the fully nonlinear solutions presented here should be examined afresh. We examine the stability of latter in this paper. Some authors have emphasized the importance of kinetic effects and hence have examined the stability using hybrid codes that treat ions kinetically. In this context, we must point out that the width of the magnetic structures as seen in *Voyager* observations is a few tens of ion gyro radii. In this regime, kinetic effects are weak and a Hall–MHD set of equations is expected to be adequate. In this paper, we have examined the stability using two codes for consistency. The two codes yield similar results. Our results show that these structures, a hole or a hump, are not quite stable. It becomes unstable with growing oscillations in the wing of the structure. MHs posses a trailing oscillation while humps have both trailing and preceding oscillations. Simultaneously, there are changes in the central structure. These results are consistent with recent observations of instability in the wings of the MHs (Burlaga et al. 2007). In the case of collision we find that if two such structures collide, they pass through each other (along with their fluctuations) with changes in their amplitude and the width. This shows that during collision there is a non-negligible energy exchange between them showing an unstable behavior.

This paper is organized as follows. In Section 2 we describe briefly the three-fluid model for the sake of completeness before extending it to a four-fluid model in Section 3. Stationary solutions are also described in Section 3. In Section 4, we describe

the simulations results. In the last section, we summarize and discuss our results.

2. THREE-FLUID MODEL

In this section, we briefly recapitulate the salient features of the three-fluid model published earlier (Avinash & Zank 2007). This will be extended to a four-fluid model in the following section. The interaction of solar wind and neutrals generates PUIs (along with already existing SWI) and a population of energetic neutrals which is distinct from the interstellar neutrals. In the three-fluid model we treat PUI and SWI as a single fluid of ions. These ions along with electrons and neutrals constitute the three fluids. As argued earlier (Avinash & Zank 2007), the electron and ion fluids are adequately described by the Hall–MHD set of equations given by

$$\frac{\partial n_p}{\partial t} + \nabla \cdot n_p \vec{v}_p = 0; \tag{1}$$

$$m_p \frac{\partial n_p \vec{u}_p}{\partial t} + m_p \nabla \cdot n_p \vec{u}_p \vec{u}_p + \nabla p_p = q n_p \vec{E} + q n_p \vec{u}_p \times \vec{B} - m_p \sigma U^* N \left(\vec{u}_p - \vec{V}\right) n_P; \tag{2}$$

$$u \frac{d}{dx}\left(p_p u^\gamma\right) = \frac{-1}{L^* \overline{V}}\left(p_p u^\gamma\right); \tag{3}$$

$$\left(\nabla p_e\right)/q n_e + \vec{E} + u_e \times \vec{B} = 0; \tag{4}$$

$$\nabla \times \vec{B} = \mu_0 \vec{J}, \nabla \times \vec{E} = -\frac{\partial \vec{B}}{\partial t}, \vec{J} = q\left(n_p \vec{u}_p - n_e \vec{u}_e\right); \tag{5}$$

$$\frac{\partial N}{\partial t} + N \vec{V} = 0; \tag{6}$$

$$\frac{\partial N \vec{V}}{\partial t} + \nabla \cdot N \vec{V} \vec{V} = \sigma_{ex} U^* N \left(\vec{u}_p - \vec{V}\right) n_p, \tag{7}$$

where n_p, $\vec{u}_p$, p_p are the proton number density, fluid velocity, and the kinetic pressure respectively while σ, U^*, N, $\vec{V}$ represent the charge exchange cross section, characteristic interaction speed, neutral number density, and the velocity, respectively. The last term on the right-hand side of Equation (2) represents the momentum input due to charge exchange. The variables E and B denote the electric and magnetic fields. The neutral dynamics is described by the last two equations.

The one-dimensional stationary time-independent solutions propagating along x can be constructed by setting $\partial/\partial t = 0$, $\nabla = \partial/\partial x$. The magnetic field at $x = -\infty$ is given by $\vec{B}_0 = B_x \hat{x} + B_{z0}\hat{z}$, where α is the angle between $\hat{x}$ and $\vec{B}_0$. As shown in Avinash & Zank (2007), the set of time-independent equations to be solved in this case are

$$u - 1 + \frac{M_N}{M_p}(\overline{V} - \overline{V}_0) = -\frac{1}{\gamma M^2}\left(\frac{p}{p_0} - 1\right) - \frac{1}{2M_\perp^2}\left\{1 - \left(b_y^2 + b_z^2\right)\right\}; \tag{8}$$

$$u \frac{db_y}{dx} = \frac{1}{L}\left[1 - M_{||}^{-2} - b_x\left(u - M_{||}^{-2}\right)\right]; \tag{9}$$

$$u \frac{db_z}{dx} = \frac{b_y}{L}\left(u - M_{||}^{-2}\right); \tag{10}$$

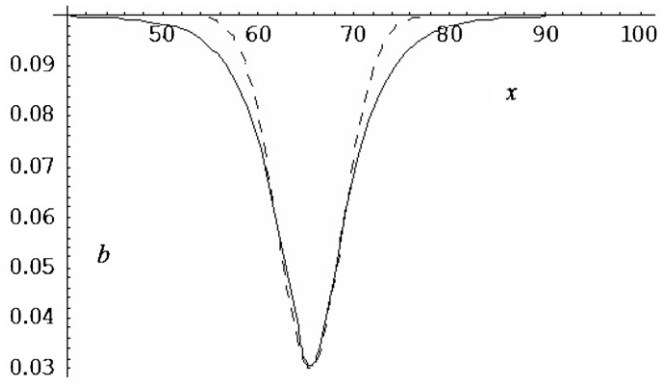

Figure 1. MH for heliosheath parameters given in the text and fitted Gaussians from the model of Avinash & Zank (2007).

$$u \frac{d}{dx}\left(p_p u^\gamma\right) = \frac{-1}{L^* \overline{V}}\left(p_p u^\gamma\right); \tag{11}$$

$$u \frac{d\overline{V}}{dx} = \frac{2}{L^*}\left(\frac{u}{\overline{V}} - 1\right)\frac{n_{p0} u_0}{N_0 V_0}, \tag{12}$$

which have used the following normalizations and definitions $p = p_e + p_i$, $p_0 = p_{p0} + p_{e0}$, p_{p0}, p_{e0} are proton and electron pressure at $x = -\infty$, $M_\perp^2 = u_0^2/V_\perp^2$, $M_{||}^2 = u_0^2/V_{||}^2$, $c_s^2 = \gamma p_0/m_p n_{p0}$, $M = c_s/u_0$, $u_{px}/u_0 = u$, $\overline{V} = V/u_0$, $b_y = B_y/B_0$, $b_z = B_z/B_{z0}$, $\left(V_\perp, V_{||}\right) = \left(B_x, B_{z0}\right)/\sqrt{\mu_0 m_p n_{p0}}$, $M_p = m_p n_{p0} u_0$, $M_N = m_N N_0 V_0$, $L = M_{||}\left(\Omega/V_\perp\right)$, $\Omega = q B_0/m_p$, and $(L^*)^{-1} = \left(\sigma U^* N_0 \overline{V}_0\right)/2\mu_0$ is the scale length associated with charge exchange. Since $M_{||} \approx 1$ and $V_\perp \approx u_0$, L is approximately equal to the proton gyro radius ρ_i. These constitute a set of five equations which can be solved to obtain five unknowns b_y, b_z, u, p, and $\overline{V}$ as functions of x. The initial values for these variables at $x = -\infty$ are $b_y = 0, b_z = 1, u = 1, p = 1$, and $\overline{V}_0 = V_0/u_0 = -\delta$ where δ is a fraction less than unity. In Figure 1, we show a dark solitary wave constructed from this model. The dashed line shows that the Gaussian is a good fit to the solution. Burlaga et al. (2006) fitted Gaussians to the MHs and humps measured in the heliosheath by the *Voyager 1* magnetometer finding good agreement. With appropriate choice of parameters in our model, we could construct holes and humps with dispersion in size ranging from approximately 30–90 ion gyro radii, as observed in *Voyager* (Burlaga et al. 2007).

Similarly we constructed solutions that resembled trains of MHs and humps using appropriate boundary conditions. These features of our solution are quantitatively consistent with the *Voyager* observations but the precise role of PUI and solar wind plasma cannot be extracted from the three-fluid model

As stated earlier, *Voyager 2* has recently crossed the termination shock (Burlaga et al. 2007) with a working plasma instrument and it has been revealed that the thermal solar wind plasma is comparatively cool downstream of the termination shock lending considerable support to the notion that PUI dynamics dominates the behavior of the structure in the heliosheath. This requires that we properly understand the relative roles of the more tenuous, more energetic PUI than the more populous but cooler thermal SWI. Accordingly, in the following section we extend our three-fluid model to incorporate the effects of PUI directly.

3. FOUR-FLUID MODEL

In the heliosheath, interstellar neutral H atoms charge exchange with SWI and produce PUI along with a population of energetic neutrals. The magnetized flow of the solar wind assimilates these ions into the bulk plasma and enforces their comotion. Because the ring distribution is unstable in velocity space, the PUI are characteristically very different from SWI. The mutual exchange of energy and momentum between these species, as well as other possible energy sources in the heliosheath such as, for example, the dissipation of the wave turbulence excited by the instability can lead to a heating of the solar wind plasma; (Zank et al. 1996a; Williams & Zank 1994; Williams et al. 1995; Matthaeus et al. 1999). This makes them nonadiabatic with different polytropic indices. Consequently, their role in the formation of magnetic structures in the heliosheath is expected to be different from each other and this should be included in a realistic and complete model.

3.1. Four Fluids

The four fluids in our model are (1) electrons, (2) PUI, (3) SWI, and (4) neutral hydrogen. The strong magnetization of the solar wind forces the comotion of PUI with bulk plasma. Hence PUI and SWI move with same fluid velocity. Since electrons are sufficiently isolated in this approximation, we take them to be adiabatic with the usual polytropic index $\gamma_e = 5/3$. The thermodynamics of PUI and SWI are a little more complicated due to their mutual energy exchange. This interaction can be described as follows. By virtue of their unstable ring distribution in velocity space, the PUIs excite a broadband of MHD waves. These may cascade toward frequencies where they can be damped by SWI. These ions are thus globally heated as they convect into the outer heliosphere. This heating of SWI is consistent with the empirical fit of Whang (1998) to the *Voyager* plasma data where a polytropic index $\gamma_s = 1.28$ was found to give a good fit between the solar wind pressure and density data. Since it is less than 5/3, it indicates a heating of SWI. This is supported in a number of studies (Williams et al. 1995, Zank et al. 1996b, Matthaeus et al. 1999) which show that dissipation of the free wave energy released by the isotropization of PUI ring distribution is possible through the nonlinear turbulent processes and this leads to a significant heating of the core solar wind protons. Further, while losing energy to SWI, PUIs are themselves energized by energy diffusion in the pre-existing turbulence (Fermi-2 energization; Isenberg 1987, Le Roux & Fichtner 1997). This nonadiabatic behavior of PUIs and SWIs can be taken into account by modeling the polytropic equation of state with an appropriately augmented index. Such an analysis has been done by Fahr & Rucinski (2002) and with appropriate modifications for our purposes we include the relevant portion of their work. We first consider the PUIs

3.2 Thermodynamics of Pick-Up Ions

A good approximation to the distribution function of PUIs has been obtained by Chalov et al. (1995, 1997) and is given by

$$f_p(v) = C(r)^{-0.33}\,(v/u)^{-1/6}\exp\left[C(r)\,(v-v_0)^{2/3}\right], \qquad (13)$$

where C is a constant, r is measured in units of AU, and $C(r) = 0.442r^{0.2}$. The density and the pressure, which are the first and the third moments of f_p, can be obtained by multiplying (13) by v and v^2 and integrating over velocity space dv yielding the following relation between these parameters

$$P_p = \alpha_c \rho_c(r) u^2, \qquad (14)$$

where α and ρ_c are functions of r and vary over the heliospheric length scale. Thus, over the scale length of the MH L, which is much smaller than heliospheric length scales, these functions can be regarded as approximately constant. PUIs can therefore be regarded as a nearly isothermal fluid with an equivalent isothermal temperature given by

$$\frac{\partial P_p}{\partial \rho_p} = \frac{P_p}{\rho_p} = \alpha_c u^2 = \kappa T_p/m_p;\;\; P_p \alpha \rho_p^{\gamma_p},\;\; \gamma_p = 1. \qquad (15)$$

This means that the energy input and output to PUIs is fine tuned in such a way that while expanding with solar wind their temperature remains constant. Detailed models of the solar wind interaction with PUI (Zank et al. 1996b; Zank 1999) show that this is the case.

3.3. Thermodynamics of Solar Wind Ions

To calculate the augmented polytropic index in the equation of state for SWIs, we may follow two approaches: (1) we may directly refer to the empirical fit of Whang (1998) or (2) solve the appropriate enthalpy equation to calculate the augmented adiabatic index. In the following, we briefly summarize both these approaches.

1. *Empirical fit.* Using the *Voyager* data over a period of 17 years (1978–1994), Whang (1998) obtained a fit of monthly averages of solar wind pressure P_s and the density ρ_s. This fit was given by $P_s \propto \rho^{\gamma_s}$ with $\gamma_s = 1.28$. The fact that this value is less than the adiabatic value 5/3 indicates that SWIs are not isolated but are constantly heated as they travel outward to distant heliosphere. As discussed by Zank et al. (1996b) and Matthaeus et al. (1999), there are several heating mechanisms for the heating of solar wind plasma, e.g., stream-shear drive, decay of shocks beyond the ionization cavity (effective $\approx$ 7–10 AU). However in the outer heliosphere the heating due to PUI is dominant.
2. *Enthalpy equation.* The equation for the enthalpy of the two-fluid system consisting of PUIs and SWIs is given by

$$\nabla\cdot\left[\frac{\gamma}{\gamma+1}\left(P_p+P_s\right)\vec{u} - \vec{u}\cdot\nabla\left(P_p+P_s\right)\right] = \beta_{ex}\left[\frac{1}{2}m_p u^2 - \kappa T_s\right] + Q_p + Q_s; \qquad (16)$$

where $\beta_{ex} = n_p n_n \sigma V_s$ is the injection rate for PUIs. For typical parameters, i.e., solar wind proton density $n_p \approx 5$ cm^{-3}, interstellar neutral density $n_n \approx 0.2$ cm^{-3}, charge exchange cross section $\sigma \approx 5\times10^{-15}$ cm^2, and solar wind velocity $V_s \approx 400$ km s^{-1}, $\beta_{ex} \approx 10^{-7}$ cm^{-3} s^{-1}. This is small as compared with ion pick-up rate in cometary environment which is $\approx 10^{-2}$ cm^{-3} s^{-1} with cometary neutral density $\approx 3\times10^4$ cm^{-3} at 11,000 km from the comet nucleus (Tsurutani & Ho 1999). The term Q_p denotes the net energy input to PUIs (losses to SWIs via wave particle interaction and gain from energy diffusion (Fermi-2 energization)). Similarly, Q_s is the net energy input to SWIs. In the case of no net energy gain or loss to the wave fields,

$Q_p + Q_s = 0$. Mass conservation of PUIs requires that $m_p\beta_{\rm ex} = \nabla\cdot(\rho_p u)$. Hence the enthalpy equation becomes

$$\nabla\cdot\left(\frac{\gamma}{\gamma-1}P_s u\right) - (u\cdot\nabla)\,P_s = -\beta_{es}kT_s - \left(\frac{\gamma}{\gamma-1} - \frac{um_p}{2kT_c}\right)\nabla\cdot(P_p u) + (u\cdot\nabla)\,P_p. \quad (17)$$

This equation is solved in the spherical geometry appropriate to heliosphere, assuming P_s, ρ_s are functions of r. Using $\frac{2u}{r} \gg \frac{du}{dr}$, $T_p \gg T_s$, and the total proton density $n = n_0\left(\frac{r}{r_0}\right)^{-2}$, Equation (17) can be cast in the form

$$\frac{dP_s}{dr} = \frac{1}{r_0}\left[-\frac{2\gamma P_s}{r} + P_{s,0}\Lambda(\alpha_1-\alpha_2)\left(\frac{r}{r_0}\right)^{-2}\right], \quad (18)$$

where $\alpha_1 = T_p/T_s, \alpha_2 = (\gamma-1)n_0m_pu^2/2P_{s,0}, \Lambda = n_0\sigma r_0$. The equation for the SWI density is $d\rho_s/dr = -2\rho_s/r$. Using this we calculate the adiabatic index of the SWIs $\gamma_s(r)$ as

$$\gamma_s(r) = \frac{\rho_s}{P_s}\frac{dP_s}{d\rho_s} = \gamma - \frac{P_{s,0}}{P_s}\frac{\Lambda}{4}(\alpha_1-\alpha_2)\left(\frac{r}{r_0}\right)^{-1}. \quad (19)$$

From this equation we obtain $\gamma_s(r)$. As shown by Fahr & Rucinski (2002), the variation of γ_s with r is not very sensitive to the values of $(\alpha_1-\alpha_2)$ or Λ. As a function of r, it starts with a value 5/3 at $r = 0$ and tends to an asymptotic value $\gamma_{s\infty} \leqslant 1.3$ for all $r > 5$ AU. This result is also consistent with Whang's empirical fit where $\gamma_s = 1.28$ in the outer heliosphere. Following these arguments we take SWI as a nonadiabatic fluid with an adiabatic index $\gamma_s = 1.28$.

3.4. Time-independent Solutions

As discussed above we describe PUIs as an isothermal fluid with a polytropic index $\gamma_p = 1$ and SWIs as a quasi-adiabatic fluid with a polytropic index $\gamma_s = 1.28$ in the four-fluid model. Further, as in the three-fluid model, we assume that all charged species are comoving with a common velocity u. The neutrals are coupled to PUIs and SWIs via charge exchange. The complete set of equations in the normalized variables is given by

$$\frac{\partial b_y}{\partial t} = \frac{\partial}{\partial x}\left[\frac{u_y}{\tan\alpha} - u_x b_y + \frac{1}{n_t}\frac{\partial b_z}{\partial x}\right]; \quad (20)$$

$$\frac{\partial b_z}{\partial t} = \frac{\partial}{\partial x}\left[\frac{u_z}{\tan\alpha} - u_x b_z - \frac{1}{n_t}\frac{\partial b_y}{\partial x}\right]; \quad (21)$$

$$\frac{\partial n_t u_x}{\partial t} = \frac{\partial}{\partial x}\left[-n_t u_x^2 - \frac{1}{M_\perp^2}\left(b_y^2+b_z^2\right) - \frac{\alpha_p^{(1-\gamma_p)}}{\gamma_p M_p^2}n_p^{\gamma_p} - \frac{\alpha_s^{(1-\gamma_s)}}{\gamma_s M_p^2}\left(n_t-n_p\right)^{\gamma_s} - \frac{1}{\gamma_e M_e^2}n_t^{\gamma}\right] - \frac{L}{L^*}\left(\frac{u_x}{V}-1\right)\frac{NV}{N_0V_0}n_t \quad (22)$$

$$\frac{\partial n_t u_y}{\partial t} = \frac{\partial}{\partial x}\left[-n_t u_y u_x + \frac{1}{M_\perp M_{||}}b_y\right] \quad (23)$$

$$\frac{\partial n_t u_z}{\partial t} = \frac{\partial}{\partial x}\left[-n_t u_z u_x + \frac{1}{M_\perp M_{||}}b_x\right] \quad (24)$$

$$\frac{\partial n_p}{\partial t} + \frac{\partial n_p u_x}{\partial x} = \frac{L}{L^*}\left[\frac{u_0^2}{U^*V_0}\right]\frac{N}{N_0}n_p u_x; \quad (25)$$

$$\frac{\partial n_s}{\partial t} + \frac{\partial n_s u_x}{\partial x} = \frac{L}{L^*}\left[\frac{u_0^2}{U^*V_0}\right]\frac{N}{N_0}n_s u_x \quad (26)$$

$$\frac{P_e}{n_e^{\gamma_e}} = \text{const}, \quad \frac{P_s}{n_s^{\gamma_s}} = \text{const}, \quad \frac{P_p}{n_p^{\gamma_p}} = \text{const}; \quad (27)$$

$$\gamma_e = 5/3, \quad \gamma_s = 1.28, \quad \gamma_p = 1, \quad (28)$$

where $n_t = n_s + n_p$ is the total proton density including the PUI and SWI densities, $\alpha_s = n_{s0}/n_{t0}$, $\alpha_p = n_{p0}/n_{t0}$ and $u_{px}/u_0 = u_x$, $u_{py}/u_0 = u_y$, $u_{pz}/u_0 = u_z$. The initial total proton density is given by $n_{t0} = n_{s0} + n_{p0}$. In the second part of the paper, we construct the time-dependent solutions by numerically integrating this set of equations. In this section, we construct the time-independent solutions by setting $\partial/\partial t = 0$ in Equations (20)–(28). In this model, there are two effects, i.e., the effect of neutrals via charge exchange and the effect of the nonadiabaticity and energy exchange among PUIs and SWIs. As can be seen in Equations (20)–(28), the charge exchange terms are ordered by the ratio L/L_*. As pointed out earlier (Avinash & Zank 2007), this ratio is small for typical parameters of the heliosheath. Thus, to lowest order in L/L_*, the charge exchange terms are small and the only dominant effect is that due to the nonadiabaticity of PUIs and SWIs. In this paper, we present time-dependent and time-independent solutions to lowest order in L/L_* where charge exchange effects are dropped while those corresponding to nonadiabaticity are retained. In this limit, the time-independent equations in a frame moving with the structure are

$$u_x\frac{db_x}{dx} = b_y\left(u_x - \frac{1}{M_{||}^2}\right); \quad (29)$$

$$u_x\frac{db_y}{dx} = -b_z\left(1-\frac{1}{M_{||}^2}\right) + 1 - \frac{1}{M_{||}^2}; \quad (30)$$

$$u_x - 1 + \frac{\alpha_p}{\gamma_p M_p^2}\left(\frac{1}{u_x^{\gamma_p}}-1\right) + \frac{\alpha_s}{\gamma_s M_s^2}\left(\frac{1}{u_x^{\gamma_s}}-1\right) + \frac{1}{\gamma_e M_e^2} \times \left(\frac{1}{u_x^{\gamma_e}}-1\right) = 1 - \frac{1}{2M_\perp^2}\left[1-\left(b_y^2+b_z^2\right)\right]; \quad (31)$$

where $M_p^{-2} = \gamma_p P_p/m_p n_{p0}u_0^2$, $M_s^{-2} = \gamma_s P_s/m_s n_{s0}u_0^2$ are the Mach numbers corresponding to the pressure of PUIs and SWIs, respectively. The boundary conditions for this set of equations are the same as that for the variables of the three-fluid model, i.e., $b_y = 0$, $b_z = 1$, $u_x = 1$. The solutions of these equations may have a maxima or a minima of the total magnetic field in the center. The necessary and sufficient conditions for the existence of solitary wave solutions of these equations have been discussed by McKenzie et al. (2001, 2004). These conditions are (1) in the neighborhood of the initial data only exponential growing eigenvalues should exist; (2) solitary wave solutions contain a maxima/or minima in variables such as b or u. The sonic point where the sound speed matches the local flow velocity, i.e., $u = (1/M_s^{2/\gamma+1})$ should not be located between the initial point and the maxima/minima (otherwise the flow would be

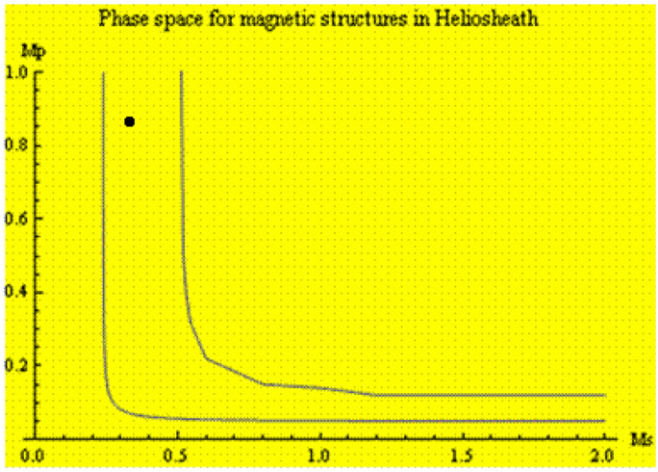

Figure 2. Phase space for magnetic structures in the heliosheath with M_s plotted along the x-axis and M_p plotted along the y-axis. Regular smooth solitary wave solutions exit only in the channel-like region between the two lines. Above and below this region the solutions are either singular or periodic. The point in the region indicates the approximate position of the heliosheath where M_p is roughly 3 to 4 times M_s.

(A color version of this figure is available in the online journal.)

choked). The second condition occurs in the construction of hump solutions. Thus, the occurrence of magnetic humps is additionally constrained by the Hall–MHD set of equations. To obtain smooth solutions, we fix M and α while M_p and M_s are varied to obtain the solutions. In Figure 2, we plot the phase space of smooth solutions in terms of M_p and M_s. The plot shows regions of smooth solutions along with regions where such solutions are not possible. Smooth solutions are possible in two channel such as regions parallel to the M_p and M_s axes. Smooth solutions are not possible when both M_p and M_s are greater than 1, being possible only when at least one of them or both are less than 1. The heliosheath ($M_p \approx 3$–$4M_s$) is represented by a point shown in the figure. This shows that the conditions in the heliosheath are conducive for the formation of stationary magnetic structures. However, the fact that MHs and humps solutions exit only in a small annular like region in the M_p-M_s phase space shows that the occurrence of these structures may not be generic in space plasmas. This may partly explain why these structures are not found to occur in other circumstances such as cometary plasmas (Brinca & Tsurutani 1989).

4. TIME-DEPENDENT SOLUTIONS

In this section, we explore the stability of the time-independent solutions computed in the previous section. This is accomplished by studying the temporal evolution of the complete set of Hall–MHD equations using the stationary solutions above as our initial conditions. As discussed earlier, the stability of DNLS soliton solutions has been studied by Baumgartel (1999), Baumgartel et al. (2003) and Buti et al. (2001a). Recently, in the context of the observations from the Cluster spacecraft, Baumgartel et al. (2005) have used the one-dimensional hybrid simulations to investigate a variety of oblique, large amplitude solitary pulses. Their study support a soliton-based interpretation of the cluster observations.

In our simulations, we take the time-independent solutions as initial conditions and then evolve them using the set of Equations (20)–(28). These equations are in the moving frame where velocities are normalized with u_0. To study the temporal evolution, we use a slightly different normalization where velocities are normalized by $V_{||}$ (defined in 2), distance by $L = B_x/\mu_0 q n_{t0} u_0$, time by $L/V_{||}$, and the number densities by the initial total proton density thus $n \equiv n_t/n_{to}$, $n_p \equiv n_p/n_{t0}$. With this normalization the set of time-dependent equations in the laboratory frame are

$$\frac{\partial b_y}{\partial t} = \frac{\partial}{\partial x}\left(\frac{u_y}{\tan\alpha} - u_x b_y + \frac{u_0}{n}\frac{\partial b_z}{\partial x}\right); \tag{32}$$

$$\frac{\partial b_z}{\partial t} = \frac{\partial}{\partial x}\left(\frac{u_z}{\tan\alpha} - u_x b_z - \frac{u_0}{n}\frac{\partial b_y}{\partial x}\right); \tag{33}$$

$$\frac{\partial n u_x}{\partial t} = \frac{\partial}{\partial x}\left[-n_t u_x^2 - \frac{1}{2}\left(b_y^2 + b_z^2\right)\tan^2\alpha - n_p^{\gamma_p}\frac{\beta_p}{\alpha_p^{\gamma_p}} - \left(n - n_p\right)^{\gamma_s}\frac{\beta_s}{\alpha_s^{\gamma_s}} - \beta_e n^{\gamma_e}\right] \tag{34}$$

$$\frac{\partial n u_y}{\partial t} = \frac{\partial}{\partial x}[-n u_y u_x + b_y \tan\alpha]; \tag{35}$$

$$\frac{\partial n u_z}{\partial t} = \frac{\partial}{\partial x}[-n u_z u_x + b_z \tan\alpha]; \tag{36}$$

$$\frac{\partial n}{\partial t} + \frac{\partial n u_x}{\partial x} = 0; \tag{37}$$

$$\frac{\partial n_p}{\partial t} + \frac{\partial n_p u_x}{\partial x} = 0; \tag{38}$$

where $\tan\alpha = B_{z0}/B_x$ and u_0 is velocity of the structure with respect to the background solar plasma. We integrate these equations in space and time to test the stability of the solitary wave structures.

4.1. Initial Conditions

The solutions of the time-independent equations are used as initial conditions in Equations (32)–(38). To obtain this set of time-independent equations we apply the transformations $\partial/\partial t = u_0 d/d\xi$, $\partial/\partial x = d/d\xi$ to the space and time operators in Equations (32)–(38). With these transforms, the time-independent equations in the laboratory frame become

$$(u_0 + u_x)\frac{db_y}{dx} = u_0 - \frac{1}{u_o} - b_z\left[(u_0 + u_x) - \frac{1}{u_0}\right]; \tag{39}$$

$$(u_0 + u_x)\frac{db_z}{dx} = b_y\left[(u_0 + u_x) - \frac{1}{u_0}\right]; \tag{40}$$

$$u_0 u_x + \beta_p\left[\left(\frac{u_0}{u_0 + u_x}\right)^{\gamma_p} - 1\right] + \beta_s\left[\left(\frac{u_0}{u_0 + u_x}\right)^{\gamma_s} - 1\right] + \beta_e\left[\left(\frac{u_0}{u_0 + u_x}\right)^{\gamma_e} - 1\right] = \frac{B_{z0}^2}{2B_x^2}\left[1 - \left(b_y^2 + b_z^2\right)\right]. \tag{41}$$

There are seven variables b_y, b_z, u_x, u_y, u_z, n_t, and n_p. Three variables, b_y, b_z, and u_x are obtained by solving Equations (39)–(41) while the rest are obtained from the following constitutive relations

$$u_y = \frac{b_y}{u_0}\tan\alpha,\ u_z = \frac{(b_z - 1)}{u_0}\tan\alpha$$
$$n_t = u_0/\left(u_0 + u_p\right),\ n_p = n_{p0}u_0/\left(u_0 + u_x\right). \tag{42}$$

The other constants in these equations are $\tan\alpha = B_{z0}/B_x$, $B_{z0}, B_x, u_0, \beta_b, \beta_s, \beta_e, \gamma_p, \gamma_e, \gamma_s, \alpha_p, \alpha_s$. The equations are integrated from $\xi = 0$ with initial conditions $u_x = 0, b_y = 0, b_z = 1$. The condition for the existence of nonoscillating smooth solutions is obtained by linearizing Equations (39)–(41) around these values with substitutions $u_x = u'_x, b_y = b'_y, b_z = 1 + b'_z$ yielding

$$\frac{B_{z0}^2}{B_x^2}\left(1 - \frac{\beta\gamma_e}{u_0^2}\right)^{-1} + 1 < u_0^2 < 1, \tag{43}$$

where $\beta = \beta_p \frac{\gamma_p}{\gamma_e} + \beta_s \frac{\gamma_s}{\gamma e} + \beta_e$. Consistent with heliosheath parameters, we choose the following values for the constants:

$$B_{z0} = 1.64, B_x = 1, u_0 = 0.96, \beta_p = 8.8, \beta_s = 2.25,$$
$$\beta_e = 2.21, \gamma_p = 1, \gamma_e = 5/3, \gamma_s = 1.28$$
$$\alpha_p = 0.091, \alpha_s = 0.909.$$

Note that on account of the higher PUI pressure the plasma beta of PUI dominates that of SWIs. Hence, the structures are mediated mainly by the PUI. This interpretation is consistent with that of Burlaga et al. (1994) who argued on the basis of the *Voyager 2* plasma and magnetic field data that pressure balanced structure in the outer heliosphere were dominated by the PUI pressure. Using these values for the constants, the solutions of the time-independent equations are constructed corresponding to (1) an MH (minima in b) moving to the left with the initial velocity u_0 shown in Figure 3(a), (2) a magnetic hump (maxima of b) moving to the left with initial velocity u_0 shown in Figure 3(b), (3) two MHs approaching each other with initial velocity u_0 shown in Figure 3(c), and (4) two magnetic humps approaching each other with initial velocity u_0 shown in Figure 3(d). The last two conditions are obtained by mirror reflection of the first two conditions about the origin $x = 0$. In these plots, the distance is normalized by L which is approximately the proton gyroradii while the time is normalized by the corresponding gyroperiod. The distance of the structure from the origin $x = 0$ in the first two cases is $\approx$250 ρ_i while the distance between two structures in the last two cases is $\approx$500 ρ_i.

4.2. Simulation Results

We evolve each of the initial conditions of Figure 3 using the set of Equations (32)–(38). The integration scheme uses periodic boundary conditions and is briefly described in the Appendix. We first consider the MH simulations. In Figure 4, we show stack plots of the evolution of a single hole moving to the left with initial velocity u_0. The plots show that the structure propagates without any perturbation till $t = 60$ (approximately 60 gyroperiods). At later times, there is a signature of instability in the tail on the right side of the structure; very low amplitude oscillations begin to grow as the structure propagates along with a slight decrease in the amplitude. This is mainly due to small changes in the local velocity of structure which, as structure propagates and no longer satisfies the condition for a nonoscillating smooth solution given by Equation (43). This probably indicates that in this instability, there is energy exchange between the magnetic and kinetic parts of the total energy of the structure. This is unlike regular soliton behavior. In Figure 5, we show stack plots of the collision of two identical counterpropagating MHs. At about $t = 80$, we see the signature of an instability in the tail. From this time onward the structures begin to overlap. At $t = 200$ the merger of the two structures is complete. From this time onward the structures reemerge. At $t =$ 300 emergence is complete. Trailing structures at this stage

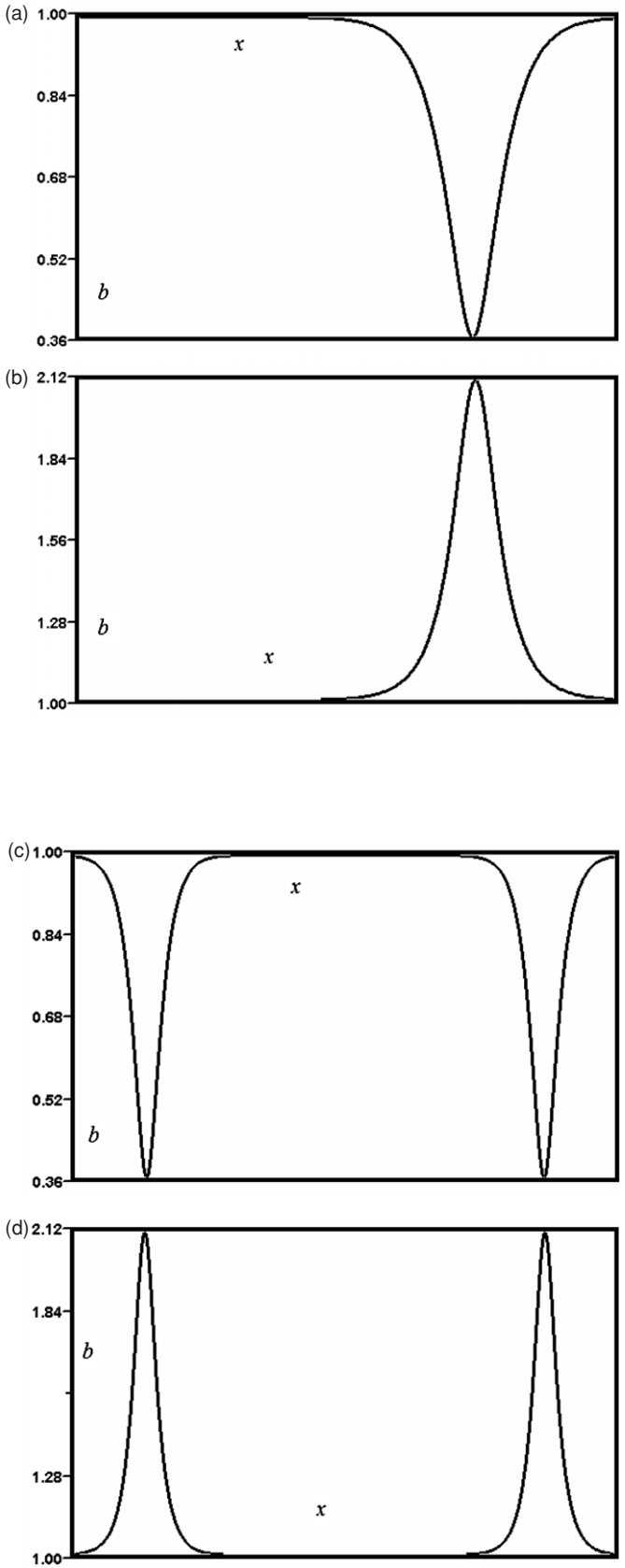

Figure 3. Initial conditions used in the simulations. The distance is plotted along the x-axis while the total magnetic field defined by $b = \sqrt{(b_y^2 + b_z^2)}$ is plotted along the y-axis. (*a*) An MH (minimum of b) moving left with initial velocity u_0. (*b*) A magnetic hump (maximum of b) moving left with initial velocity u_0. (*c*) Two MHs approaching each other with initial velocity u_0. (*d*) Two magnetic humps approaching each other with initial velocity u_0.

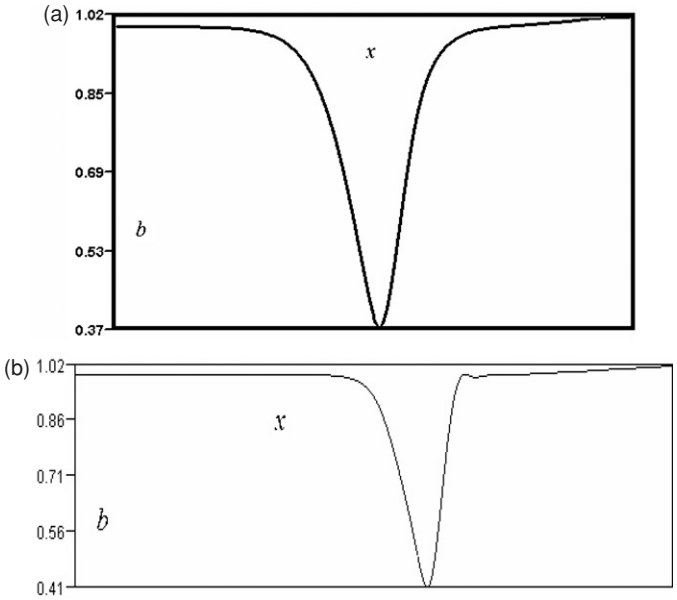

Figure 4. Propagation of a single hole to the left with initial velocity u_0 (*a*) at $t = 60$ the hole propagates without major distortion; (*b*) instability in the tail of the left of the hole at later times accompanied by an increase in the amplitude.

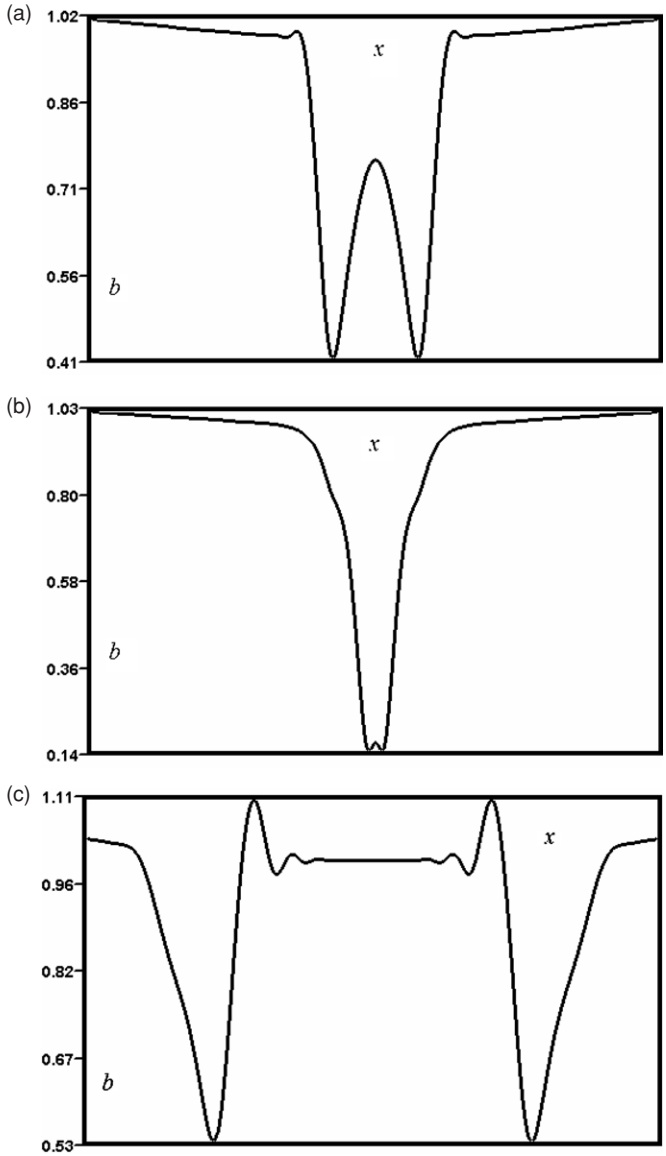

Figure 5. Collision of MHs approaching each other with initial velocity u_0: (*a*) small oscillations growing in the tail region of two holes at $t = 80$; (*b*) complete overlap of the two holes at $t = 200$; (*c*) re-emergence of two holes with oscillations in between at $t = 300$.

indicate that the structures coming from the right are now on the left and vice versa. However, the amplitudes and width of the structures before and after the collision are different. This indicates that during the collision there is considerable energy exchange between the structures. This behavior is unlike soliton which preserve their structure with very little energy exchange in collision.

Next we turn to the simulation of magnetic humps with parameters similar to the hole simulation given in Equation (43). The picture that emerges from this simulation is as follows. In Figure 6, we show stack plots of the results of the evolution of a single magnetic humps moving to left with an initial velocity u_0. It develops instability with growing fluctuations on the wings of the central structure. Typically, the preceding fluctuations are short scale while the trailing fluctuations are long scale. Simultaneously, the amplitude grows while the width of the structure decreases slightly. These changes indicate an exchange of magnetic and kinetic energy in the structure. They continue till the end of run at $t = 120$ with out saturation. Figure 7 shows the collision of two identical counterpropagating humps. Around $t = 40$, oscillation begin to grow in the tail region of the two humps. These propagate till $t = 120$ when they begin to overlap. At $t = 160$, the overlap is complete and the plot shows a single structure. The postcollision plot at $t = 200$ shows that the amplitudes and the width of the central structures before and after the collisions are different indicating energy exchange between them in collision. Again, by comparing the positions of preceding and trailing fluctuations before and after the event we conclude that the structures have gone through each other.

These results are partially consistent with those of Baumgartel (1999) on the stability of DNLS solitons. In his simulation solutions of DNLS equation are evolved using Hall–MHD equations. His results show that in the collision of two bright DNLS soliton, the structures coming out of the collision are different from those going in and hence there is considerable energy exchange between them. This part of his simulation is consistent with our results on the collision of two humps shown here. However, the dark DNLS solutions in Baumgartel (1999) simulation go through each other with out any change of shape. This is in contrast with our simulations here on humps. One reason for this difference is that dark DNLS solitons are solutions of the DNLS equation under the condition when dispersion in the wave balances the nonlinearity. This aspect is presumably preserved by Hall–MHD equations at least for dark solutions. Our solitary wave solutions on the other hand are general solutions of MHD equations without any such condition. Hence there is no a priori reason why these solutions should preserve their structure in single propagation or in collision.

Our simulation results are consistent with recent analysis of MHs by Burlaga et al. (2007) regarding *Voyager 1* ob-

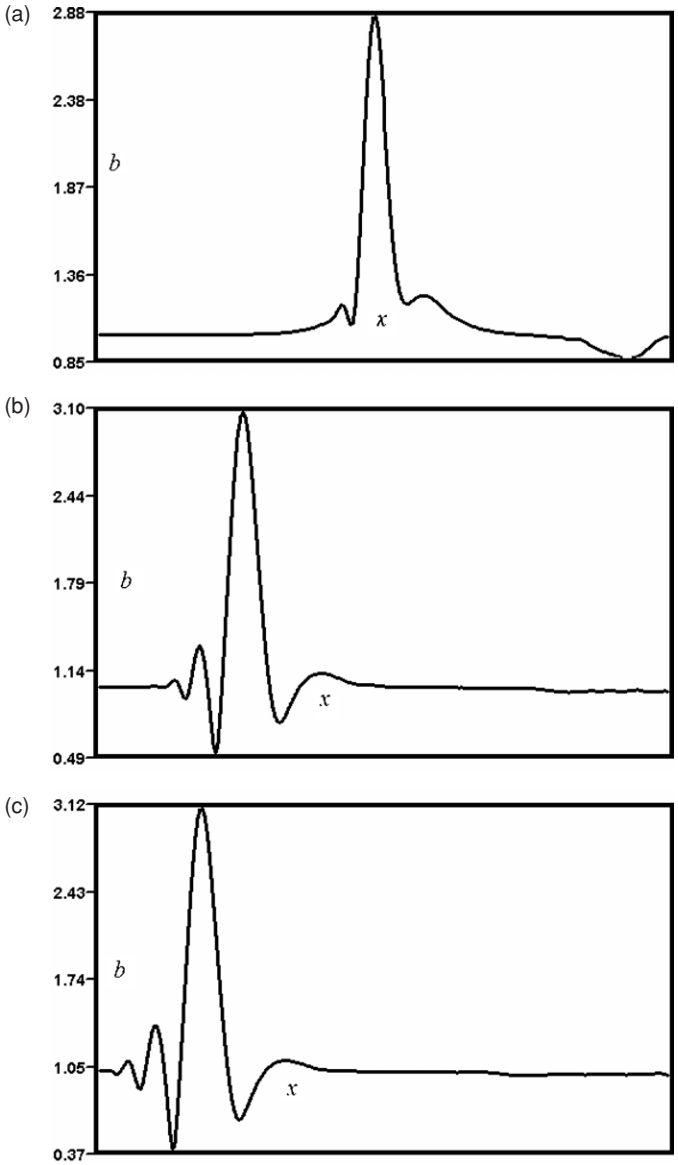

Figure 6. Propagation of single magnetic hump: (*a*) $t = 50$, (*b*) $t = 100$, and (*c*) $t = 200$. These plots show growing oscillations in the tail region of the structure. Typically the preceding oscillations are short scale while the trailing oscillations are long scale in character.

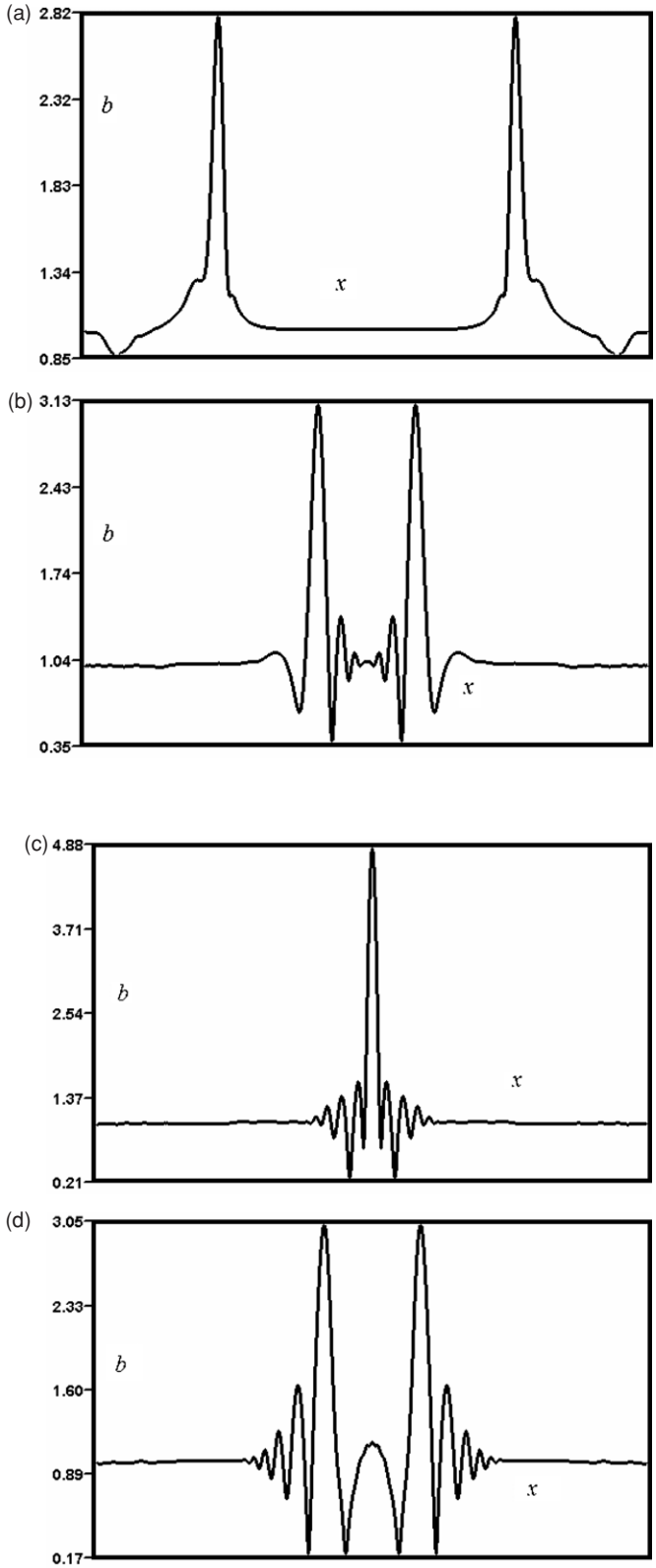

Figure 7. Collision of two magnetic humps: (*a*) $t = 40$ oscillations begin to grow in the tail region of the two humps; (*b*) $t = 120$ structures begin to overlap; (*c*) $t = 160$ shows a complete overlap; (*d*) at $t = 200$ the postcollision plot shows that amplitude and width before and after are different indicating energy exchange between the structures.

servations from the unipolar region in the heliosheath. This analysis shows that though the main structure is well described by a Gaussian-shaped structure fluctuations are invariably present in the wings. Such fluctuations have earlier been observed in MHs at 1 AU (Fitzenreiter & Burlaga 1978). The presence of these oscillations could be related to instability (Burlaga et al. 2007). In our simulations of magnetic humps and holes we actually see the evidence of this instability. Further work is required to identify the exact nature and mechanism of this instability. This will be the subject of a future paper.

5. SUMMARY AND DISCUSSIONS

Recently, we have proposed a realistic three-fluid model (Avinash & Zank 2007) for magnetic structures observed in the heliosheath which is based on the work of Mckenzie et al. (2001, 2004). The three fluids in the model are electrons, heliosheath

ions, and neutrals. Stationary, time-independent solutions of this model consisting of holes, humps, trains of holes, and humps etc. were found with width of a few tens of ion gyroradii, large magnetic maxima/minima, and oblique angles of propagation, and shapes that were well approximated by Gaussians. These are consistent with *Voyager* observations. In the first part of the present work, we extend the three-fluid model to a four-fluid model consisting of electrons, PUIs, SWIs, and neutral hydrogen. The PUIs are generated by neutrals via charge exchange with SWI. The kinetic pressure of PUI is nearly three to four times the pressure of SWI. Hence these are more suited to mediate small-scale structures in the heliosheath such as shocks, MHs/humps etc. The constant energy exchange between these two fluids drives them nonadiabatic. The modified adiabatic index γ, may be calculated by solving the corresponding enthalpy equation. The solution shows that PUIs are nearly isothermal ($\gamma = 1$), while SWIs have $\gamma \approx 1.25$. In the four-fluid model, these effects are captured by including a modified equation of state for PUI and SWI. The phase space of time-independent solutions in terms of the Mach numbers of PUI and SWI is constructed to delineate the parameter space which allows structure formation in the heliosheath. Since the pressure of PUIs dominates over that of SWIs and electrons the former predominantly mediates the small-scale structure in the heliosheath. In the second part of our work, we examine the stability of the time-independent structure computed in the first part by evolving them using a full set of modified Hall–MHD equations. The evolution is examined using two codes, a pseudo-spectral code and a code based on a finite difference scheme, and the results were cross-checked. Our results show that a single structure, a hole, or a hump, is not quite stable. It becomes unstable and develops growing oscillations in the wings. MHs have trailing oscillations while humps have trailing as well as preceding oscillations. Concomitantly, there are changes in the central structure. The excitation of growing oscillations is probably due to local changes in the velocity which indicates that the instability is due to exchange between the magnetic and kinetic parts of the total energy. In collisions of two such structures, they pass through each other (along with their fluctuations) with non-negligible energy exchange between them. Our time-dependent analysis thus shows that the solitary wave structures predicted by Mckenzie et al. (2001, 2004) and Avinash & Zank (2003) are unstable.

These simulation results are also consistent with the recent analysis of MHs reported by Burlaga et al. (2007). In that analysis, it is shown that though Gaussian shape is a good approximation to the MH, oscillations are always present in the tail, which could be related to instability. In our simulation, we see the evidence of this instability. The exact physical mechanism and the nature of this instability require further work which will be reported in a future publication. Another problem of which has not been addressed in this paper and by other authors hitherto is the propagation of structures in inhomogeneous plasmas. Since the heliosheath plasma is invariably inhomogeneous this problem is of considerable importance and will help in identifying the nature of the instability.

APPENDIX

The spectral and finite difference codes integrate the dynamical set of Equations (32)–(38) in one dimension. The spatial discretization in the spectral code uses a discrete Fourier representation of modes, while the Runge–Kutta 4 method is used for the temporal integration. Periodic boundary conditions are employed. The code ensures conservation of total energy and mean fluid density per unit time in the absence of charge exchange and external random forcing. Additionally, $\nabla \cdot \vec{B} = 0$ is satisfied at each time step. The code is initialized with steady state (with respect to a frame moving with a characteristic speed u_0) localized solutions of the physical variables. Time evolution is followed for a long time (many nonlinear turnover periods) in a computational box of length 500–1000 Δx (where Δx is the distance between two fixed computational grids).

REFERENCES

Avinash, K., & Zank, G. P. 2007, Geophys. Res. Lett., 34, L05106
Baumgartel, K. 1999, J. Geophys. Res., 104, 28295
Baumgartel, K., Sauer, K., & Dubinin, E. 2003, Geophys. Res. Lett., 30, 1761
Baumgartel, K., Sauer, K., & Dubinin, E. 2005, Nonlin. Process. Geophys., 12, 291
Brinca, A. L., & Tsurutani, B. T. 1989, J. Geophys. Res., 94, 13565
Burlaga, L. F., & Lemaire, J. F. 1978, J. Geophys. Res., 83, 5157
Burlaga, L. F., Ness, N. F., & Acuña, M. H. 2007, J. Geophys. Res. A, 112, 07106
Burlaga, L., Ness, N., Belcher, J., Szabo, A., Isenberg, P., & Lee, M. 1994, J. Geophys. Res., 99, 21511
Burlaga, L. F., et al. 2006, ApJ, 642, 584
Buti, B., Goldstein, B. E., & Liewer, P. C. 2001a, Geophys. Res. Lett., 28, 91
Buti, B., Tsurutani, B. T., Neugebauer, M., & Goldstein, B. E. 2001b, Geophys. Res. Lett., 28, 1355
Chalov, S. V., Fahr, H. J., & Izmodenov, V. 1995, A&A, 304, 609
Chalov, S. V., Fahr, H. J., & Izmodenov, V. 1997, A&A, 320, 659
Chandrasekhar, S., Kaufman, A. N., & Watson, K. M. 1958, Proc. R. Soc. Lond. A, 245, 435
Erdos, G., & Balogh, A. 1996, J. Geophys. Res., 101, 1
Fahr, H. J., & Rucinski, D. 2002, Nonlin. Process. Geophys., 9, 377
Fitzenreiter, R. J., & Burlaga, L. F. 1978, J. Geophys. Res., 83, 5579
Franz, M., et al. 2000, J. Geophys. Res., 105, 12725
Hasegawa, A. 1969, Phys. Fluids, 12, 2642
Isenberg, P. A. 1987, J. Geophys. Res., 92, 1067
Kennel, C. F., et al. 1988, Phys. Fluids, 31, 1949
Kivelson, M. G., & Southwood, D. J. 1996, J. Geophys. Res., 101, 17315
Le Roux, J. A., & Fichtner, H. 1997, J. Geophys. Res., 102, 17365
Luhr, H., & Klocker, N. 1987, Geophys. Res. Lett., 14, 186
Matthaeus, W. M., Zank, G. P., Smith, C. W., & Oughton, S. 1999, Phys. Rev. Lett., 82, 3444
McKenzie, J. F., et al. 2001, J. Plasma Phys., 65, 213
McKenzie, J. F., et al. 2004, J. Plasma Phys., 70, 431
Neugebauer, M., et al. 2001, J. Geophys. Res., 106, 5635
Russell, C. T., et al. 1987, Geophys. Res. Lett., 14, 644
Stasiewicz, K., Seyler, C. E., Mozer, F. S., Gustafsson, G., Pickett, J. S., & Popielawska, B. 2001, J. Geophys. Res., 106, 29503
Sugiura, M., Skillman, T. L., Ledley, B., & Heppner, J. P. 1969, Eos Trans. AGU, 50, 278
Treumann, R., Brostrom, L., LaBelle, J., & Sckopke, N. 1990, J. Geophys. Res., 95, 19099
Tsurutani, B., & Ho, C. 1999, Rev. Geophys., 37, 517
Tsurutani, B. T., et al. 1982, J. Geophys. Res., 87, 6060
Tsurutani, B. T., et al. 1999, Nonlin. Process. Geophys., 6, 229
Tsurutani, B. T., et al. 2002, Geophys. Res. Lett., 29, 86
Tsurutani, B. T., et al. 2005, Nonlin. Proces. Geophys., 12, 321
Turner, J. M., et al. 1977, J. Geophys. Res., 82, 1921
Vasquez, B. J., & Hollweg, J. V. 1999, J. Geophys. Res., 104, 4681
Violante, L., et al. 1995, J. Geophys Res., 100, 12,047
Whang, Y. C. 1998, J. Geophys. Res., 103, 17419
Williams, L., & Zank, G. 1994, J. Geophys. Res., 99, 19229
Williams, L. L., Zank, G. P., & Matthaeus, W. H. 1995, J. Geophys. Res., 100, 17,059

Winterhalter, D., Neugebauer, M., Goldstein, B. E., Smith, E. J., Tsurutani, B. T., Bame, S. J., & Balogh, A. 1995, Space Sci. Rev., 72, 201
Winterhalter, D., Smith, E., Neugebauer, M., Goldstein, B., & Tsurutani, B. 2000, Geophys. Res. Lett., 27, 1615
Winterhalter, et al. 1994, J. Geophys. Res., 99, 371
Zank, G. P. 1999, Space Sci. Rev., 89, 413
Zank, G. P., Matthaeus, W. H., & Smith, C. W. 1996a, J. Geophys. Res., 101, 17093
Zank, G. P., et al. 1996b, J. Geophys. Res., 101, 457
Zurbuchen, T. H., & Jokipii, J. R. 2002, EOS, 83, 499
Zwan, B., & Wolf, R. 1976, J. Geophys. Res., 81, 1636